IEEE Access
Multidisciplinary | Rapid Review | Open Access Journal

Received April 13, 2021, accepted April 30, 2021, date of publication May 11, 2021, date of current version May 21, 2021.

Digital Object Identifier 10.1109/ACCESS.2021.3078895

Antenna Element Space Interference Cancelling Radar for Angle Estimations of Multiple Targets

RAN SUN[1], (Member, IEEE), JUNICHIROU SAKAI[1], KOUHEI SUZUKI[1], JIAYING ZHENG[1], SHIGEKI TAKEDA[1], (Member, IEEE), MASAHIRO UMEHIRA[1], (Member, IEEE), XIAOYAN WANG[1], (Senior Member, IEEE), AND HIROSHI KURODA[2]

[1]College of Engineering, Ibaraki University, Hitachi 316-8511, Japan
[2]Hitachi Astemo Ltd., Hitachi 312-8503, Japan

Corresponding author: Ran Sun (ran.sun.es@vc.ibaraki.ac.jp)

ABSTRACT This paper focuses on estimating the angle and size of different-sized targets using a radar system that estimates the angles of trucks, vehicles, bicycles, and pedestrians. The problem is that the presence of a sidelobe from the larger target degrades the accuracy of estimating the angle and size of the smaller target in multiple target detection. In this paper, a novel scheme, called antenna element space interference cancelling (AIC), is proposed for reducing the influence of the sidelobe. The performance of the proposed AIC radar system was evaluated through both computer simulations and experiments. The simulation results show that the proposed AIC radar system can estimate the angles of smaller targets within a 1-degree error, and the size estimation error is 1 dB. The experimental results also show that the proposed AIC radar is effective in detecting smaller targets that cannot be detected with traditional methods due to the sidelobes of larger targets.

INDEX TERMS FMCW radar, millimeter-wave, antenna element space interference cancelling, MIMO, sidelobe influence, angle estimation, size estimation.

I. INTRODUCTION

With the continuous growth of vehicle ownership, road traffic safety and collision avoidance have become more important. Recently, frequency-modulated continuous wave (FMCW) radar systems using the millimeter-wave frequency band have been widely used in autonomous driving systems or advanced driver assistant systems (ADASs) [1]. Compared with camera sensors, millimeter-wave radars can be smaller in size, simpler in structure, lower in cost [2], and more robust to weather [3] and curved roads [4]. Four basic pieces of information: range, velocity, angle, and size, are necessary for radar target recognition/imaging. Many studies have been carried out to improve the resolution and accuracy of the estimation of this information, such as structure enhancement for radar implementation [5]–[8], multiple-input multiple-output (MIMO) radar [9]–[12], virtual antennas [13], and multiple signal classification (MUSIC) algorithms [14]. In practical automotive radar systems, multiple target imaging capabilities are essential. Cluster recognition [15]–[17] and human/pedestrian detection are required [18], [19].

The associate editor coordinating the review of this manuscript and approving it for publication was Tutku Karacolak.

In multiple target imaging, the presence of sidelobes and grating lobes affects the accuracy of the estimations of the angle and size. In particular, the influence of sidelobes is high when the targets are of different sizes. We focus on estimating the angle and size of different-sized targets using a system that estimates the angles among trucks, vehicles, bicycles, and pedestrians. In particular, the radar cross-sectional areas (RCSs) of pedestrians are quite smaller than those of vehicles or cars. Thus, the presence of sidelobes for a large target, such as a car or a truck, degrades the accuracy of estimating the angle and size of the small target. We call the influence of the sidelobes antenna element space interference. For sidelobe suppression, one of the methods is to increase the sampling number. In two-dimensional range-velocity FFT in the millimeter-wave automotive FMCW radars [3], it is easy to increase the sampling number by modifying the software settings for the chirp signal. However, in angle estimation, a higher sampling number requires more physical receiving antennas and more radio frequency (RF) circuits. Thus, we need a signal processing method to solve this sidelobe influence in the millimeter-wave automotive FMCW radars.

Some studies have reduced the grating-lobe interference [20]–[22]. They can also be applied to sidelobe suppression.

Moreover, artificial intelligence (AI) has also been investigated for use in target recognition [23]–[26]. However, the complexity of these methods is too high. For road traffic, a simpler method is needed.

A novel simple cancellation scheme, called antenna element space interference cancelling (AIC), has been proposed for reducing the influence of sidelobes, reported in [28] as an extended summary. AIC is a successive interference cancellation (SIC)-like interference cancellation scheme. SIC is a cancellation technique widely used for wireless data transmission [29], [30]. It decodes the stronger signal first, then subtracts the decoded stronger signal from the received signal, and finally decodes the remaining signal as the weaker signal. In radio astronomy, there is a famous cancellation scheme called the CLEAN algorithm, which was proposed by Jan Högbom in 1974 [31]. CLEAN has been further developed to use for de-nosing [32], [33], reflection cancellation [34] and sidelobe suppression [35], [36] in various kinds of radars. However, the cancellation is usually executed in the dirty beam map, which can be regarded as the spatial spectrum. Its computational complexity depends on the sampling number of the spatial spectrum. To ensure the angle estimation accuracy, every sampling point of the spatial spectrum requires to execute a subtraction. This processing makes the cancellation scheme complex. A more suitable and simpler cancellation scheme for the millimeter-wave automotive FMCW radar is required.

Our proposed AIC scheme executes the cancellation scheme in the antenna element space, which is one step before the spatial spectrum. The computational complexity of AIC depends on the number of antenna elements. Due to the size of the radar and the cost of the RF circuit, the number of antenna elements used in general millimeter-wave automotive FMCW radars is limited to only 8 - 12, even when considering MIMO radar; this makes the computational complexity for the cancellation in the antenna element space lower than that in the spatial spectrum. In FMCW radars, it is easy to obtain a received signal vector (a plane wave reflected from targets) from the peak detected by two-dimensional range-velocity FFT [3]. Thus, a nearly perfect replica signal reflected from the larger target can be generated. First, the proposed AIC radar system estimates the angle and size of the larger target. Second, the proposed system generates a replica signal vector at the estimated angle of the larger target. Third, the proposed system subtracts the replica signal vector from the original received signal vector (cancels the replica in the antenna element space). Finally, the proposed system estimates the angle and size of the smaller target from the remaining signal vector. Thus, we demonstrate and validate in this paper that the smaller target can be estimated more accurately by cancelling the interference of the larger target. CLEAN and our proposed AIC schemes are similar to each other because they are both based on successive cancellation processing. However, as mentioned above, the proposed method is more suitable and has more natural processing for the recent millimeter-wave automotive FMCW radar. In this paper, we investigate the performance of the proposed AIC radar system through both computer simulations and experiments.

The rest of this paper is organized as follows. In section II, the structure of our proposed AIC radar system is presented. The performance of the proposed AIC radar system is evaluated by computer simulations and experiments. The simulation results are given in section III. The experimental results are shown in section IV. In section V, the conclusions of this paper are given.

II. PROPOSED AIC RADAR SYSTEM

Figure 1 illustrates the system structure of the proposed AIC radar system. The proposed system is planned to be introduced into vehicles as a vehicle-borne radar application for detecting different-sized targets simultaneously, such as pedestrians, bicycles, vehicles and trucks, as shown in Fig. 2.

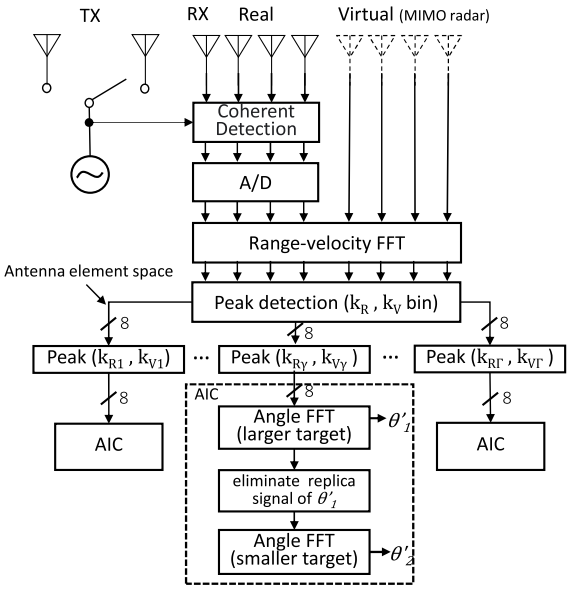

FIGURE 1. System structure of the proposed AIC radar system.

Basically, the radar system transmits radio waves, and then, the array antennas receive the reflected waves from the targets. In this paper, the use of a MIMO radar that has two transmitting antennas and four receiving antennas is assumed.

In this case, the received signals can be understood as the received signals from eight-element receiving antennas. The detection of ranges, velocities, sizes, and angles can be realized with digital signal processing. In detail, the received signals are transformed to the frequency domain signals using a two-dimensional fast Fourier transform (FFT). This is called the range-velocity FFT, which is used to detect ranges and velocities. For angle estimation, we use a beam-forming technique (angle FFT). Most targets can be distinguished by the two-dimensional range-velocity FFT. However, some targets in the same range-velocity bin can only be distinguished by angle FFT; for example, the targets are set at symmetrical

FIGURE 2. Vehicle-borne radar application for detecting pedestrians, bicycles, vehicles and trucks.

angles in a row. In the conventional system, all the angles of the targets in the same range-velocity bin are estimated at once. However, when the targets are of different sizes, the sidelobes of the larger target degrade the accuracy of estimating the angle and size of the smaller target. Thus, we add the proposed AIC scheme to the radar system.

Since most targets can be distinguished by the two-dimensional range-velocity FFT, we detected the angles of arrival from two different-sized targets in the same range. Figure 3 shows a received plain-wave sample. The received signal vector in the FFT bin of the γ-th peak can be defined as

$$\boldsymbol{x}(k_{R\gamma}, k_{V\gamma}) = h_1\boldsymbol{a}(\theta_1) + h_2\boldsymbol{a}(\theta_2) + \boldsymbol{n} \tag{1}$$

where k_R and k_V are indexes of the range and velocity bins, respectively. For simplicity, the subscript γ is omitted in the definitions hereafter. $\boldsymbol{x}(k_{R\gamma}, k_{V\gamma}) = [x_1, x_2, \cdots, x_N]^T$, where N is the number of receiving antennas and $(\cdot)^T$ denotes the transpose operator. h_1 and h_2 are the coefficients of two incident waves, which can be defined as complex numbers,

$$h_i = A_i \exp(j\phi_i) \quad (i = 1, 2) \tag{2}$$

where j denotes an imaginary unit; A_i is the amplitude, which is proportional to the RCS of the target; and ϕ_i represents the phase of the received signal. $\frac{|h_1|}{|h_2|}$ is their amplitude ratio, and $|h_1| > |h_2|$ is assumed.

θ_1 and θ_2 are the angles of the two incident waves. $\boldsymbol{a}(\cdot)$ is a steering vector. $\boldsymbol{n}$ denotes a noise vector. For a plane wave, the steering vector for the i-th incident wave is given by

$$\boldsymbol{a}(\theta_i) = \left[e^{j\frac{2\pi}{\lambda}d_1 \sin\theta_i}, e^{j\frac{2\pi}{\lambda}d_2 \sin\theta_i}, \cdots, e^{j\frac{2\pi}{\lambda}d_N \sin\theta_i}\right]^T \tag{3}$$

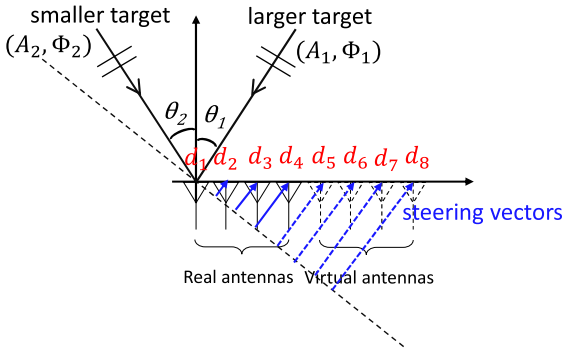

FIGURE 3. A received plain-wave sample of MIMO radar when detecting two different-sized targets.

where λ is the wavelength and $d_m (m = 1, 2, \cdots, N)$ denotes the location of the m-th antenna element.

The coefficient, h_1, can be estimated as

$$h_1' = \frac{1}{N}\boldsymbol{a}^H(\theta_1')\boldsymbol{x}(k_{R\gamma}, k_{V\gamma}) \tag{4}$$

where $(\cdot)^H$ represents the conjugate transpose of a complex matrix. θ_1' is the angle of the larger target estimated by the beamformer method as [37], [38]

$$P_{BF}(\theta) = \frac{\boldsymbol{a}^H(\theta)\boldsymbol{R}_{xx}\boldsymbol{a}(\theta)}{\boldsymbol{a}^H(\theta)\boldsymbol{a}(\theta)} \tag{5}$$

where $\boldsymbol{a}(\theta)$ is a steering vector for an arbitrary angle, θ. $\boldsymbol{R}_{xx}$ is the correlation matrix of the signal vector $\boldsymbol{x}(k_{R\gamma}, k_{V\gamma})$, which is given by

$$\boldsymbol{R}_{xx} = \boldsymbol{x}(k_{R\gamma}, k_{V\gamma})\boldsymbol{x}^H(k_{R\gamma}, k_{V\gamma}). \tag{6}$$

Thus, the signal vector after AIC, $\hat{\boldsymbol{x}}(k_{R\gamma}, k_{V\gamma})$, is given by

$$\hat{\boldsymbol{x}}(k_{R\gamma}, k_{V\gamma}) = \boldsymbol{x}(k_{R\gamma}, k_{V\gamma}) - h_1'\boldsymbol{a}(\theta_1'). \tag{7}$$

The AIC scheme can be summarized as follows:

1) estimate the angle of the larger target,
2) estimate the coefficient of the larger target and create a replica signal of the larger target,
3) cancel the larger target signal by using the replica from the original received signal vector, and
4) estimate the angle of the smaller target.

If the radar receives more than two waves, the system iterates the above scheme, which can be called the successive AIC scheme. For each iteration, a threshold of the received radio wave power is used to determine the presences of targets. The AIC scheme is iterated until no targets are detected.

III. SIMULATION RESULTS

We analyze the estimation performance of the proposed AIC radar system through computer simulations. Three different-sized targets are assumed to be used in the simulation, and the RCSs of these targets are set as 2.37 dBSm, 14.4 dBSm, and 20.3 dBSm, which can be regarded as pedestrians, vehicles, and trucks, respectively. The operating frequency

is set to 77 GHz, corresponding to a wavelength of approximately 4 mm. This causes the angle and size estimation performances to be seriously affected by the setting angles, amplitude ratios, and phases. We first present some representative cases of the angle and size estimations to confirm these influences.

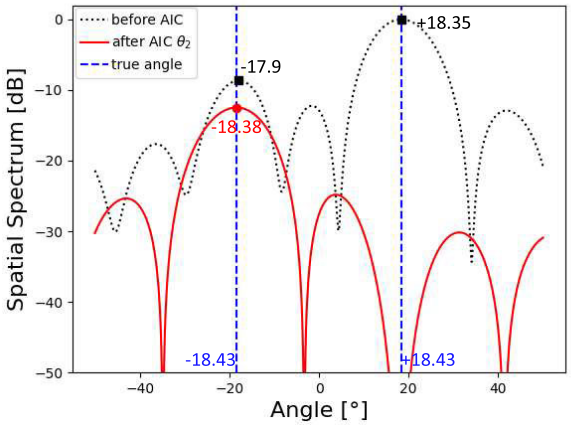

FIGURE 4. Simulation result of the proposed AIC radar when detecting a pedestrian (left, RCS is 2.37 dBSm) and a vehicle (right, RCS is 14.4 dBSm) at ±18.43° true angles without phase difference.

Figure 4 depicts the simulation result of the proposed AIC radar system when detecting a pedestrian (left) and a vehicle (right). The true angles are set as ±18.43°. The true amplitude ratio between the smaller target and the larger target is 2.37 − 14.4 = −12.03 dB, which is a metric for size estimation.

Note that the spatial spectrum in the graph is normalized by the larger target. The simulation in Fig. 4 does not consider the phase, which means that the phases of those targets' received signals are both 0 rad. We can see that the angle of the right larger target can be estimated quite accurately as +18.35° in this case. The angle estimation before AIC of the left smaller target is also not bad at −17.9°, but the received power difference, which should be the same as the true amplitude ratio, is estimated to be -8.6 dB with a 3 dB error. As we mentioned, it is caused by interference from a sidelobe of the larger target. After AIC, the angle of the smaller target can be estimated to be −18.38°, and the received power difference becomes −12.4 dB.

Fig. 5 and Fig. 6 also show the simulation results when detecting a pedestrian and a vehicle without a phase difference. In Fig. 5, the true angles are set as small angles, ±15°. Before AIC, the angle of the right larger target is estimated quite accurately to be +15.46°, but the left smaller target is estimated to be −18.92° with a 3° error. The received power difference is estimated to be −9.8 dB with a 2 dB error. After AIC, the angle of the left smaller target is estimated to be −15.32°, and the received power difference becomes −12.3 dB.

In Fig. 6, the true angles are set as large angles, ±32°. Before AIC, the angle of the right larger target is estimated to be +32.23°, and the left smaller target is estimated to

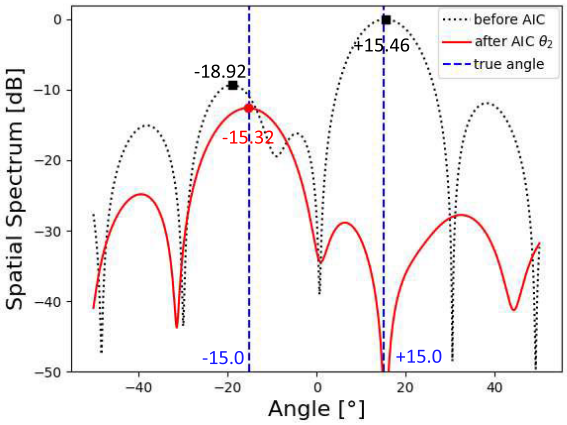

FIGURE 5. Simulation result of the proposed AIC radar system when detecting a pedestrian (left, RCS is 2.37 dBSm) and a vehicle (right, RCS is 14.4 dBSm) at ±15° true angles without phase difference.

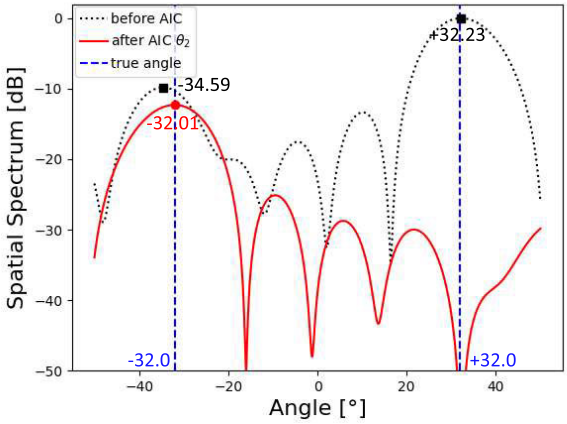

FIGURE 6. Simulation result of the proposed AIC radar system when detecting a pedestrian (left, RCS is 2.37 dBSm) and a vehicle (right, RCS is 14.4 dBSm) at ±32° true angles without phase difference.

be −34.59° with a 2° error. The received power difference is estimated to be −9.8 dB with an error of approximately 2 dB. After AIC, the errors can be reduced. The angle of the left smaller target becomes −32.01°, and the received power difference expands to −12.3 dB.

Figure 7 presents the simulation result at true angles ±32° when detecting a pedestrian and a truck. Thus, the true received power difference between the smaller target and the larger target expands to 2.37 − 20.3 = −17.93 dB. Before AIC, the angle of the larger target is estimated as +32.12°, but the angle of the smaller target is estimated to be +10.0° with quite a large error. We can see that because of the large received power difference between the pedestrian and the truck, the peak of the sidelobe from the larger target has been selected to estimate the smaller target. After AIC, the angle of the smaller target is modified to −32.01°, and the received power difference becomes −18.14 dB (true −17.93 dB).

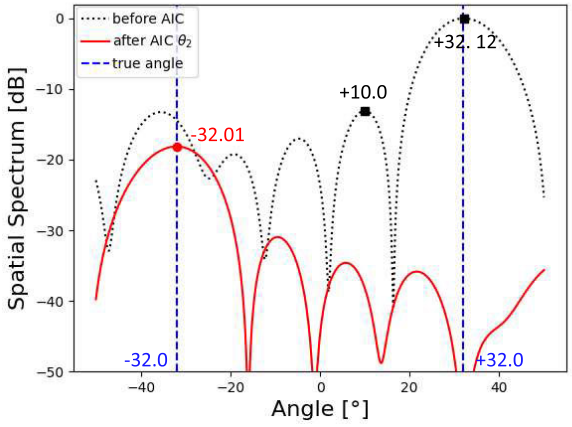

FIGURE 7. Simulation result of the proposed AIC radar system when detecting a pedestrian (left, RCS is 2.37 dBSm) and a vehicle (right, RCS is 20.3 dBSm) at ±32° true angles without phase difference.

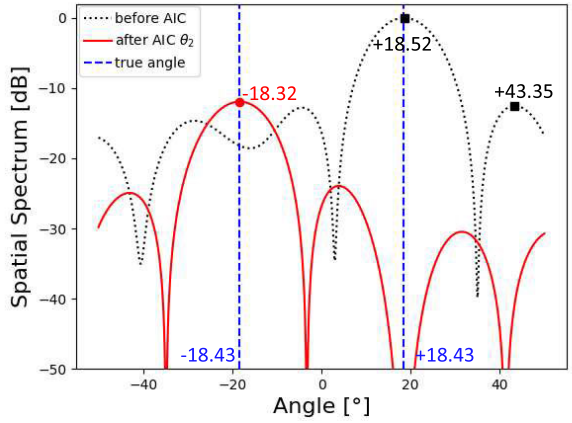

FIGURE 8. Simulation result of the proposed AIC radar system when detecting a pedestrian (left, RCS is 2.37 dBSm) and a vehicle (right, RCS is 14.4 dBSm) at ±18.43◦ true angles with phases $-8/9\pi$ rad and 0 rad.

To conclude, the accuracy of the angle estimation depends on the true angles and the target size differences, and the error can be reduced by the proposed AIC radar system.

Moreover, the phase difference also affects the angle estimation performance. Figure 8 shows the worst case of the simulation result when detecting pedestrians and vehicles at true angles ±18.43°. The phases of the signals received from the smaller target and the larger target are set as $-8/9\pi$ rad and 0 rad, respectively. Before AIC, the angle of the larger target is estimated to be +18.52°, but the angle of the smaller target is estimated to be +43.35°. We can see that there is a concave shape around the true angle of the smaller target because the received larger target signal by the sidelobe cancels the received smaller target signal by the mainlobe when the phase difference is $-8/9\pi$ rad. After AIC, the angle of the smaller target is estimated to be −18.32°, and the received power difference becomes −11.9 dB (true −12.03 dB). Thus, the proposed AIC scheme effectively reduces the influence of the phase difference.

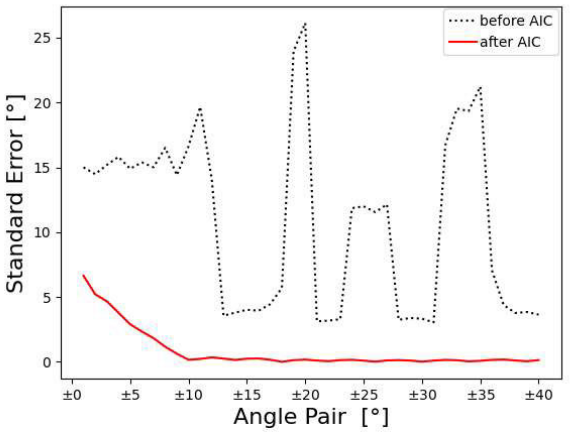

FIGURE 9. Standard error versus angle pair of the proposed AIC radar system when detecting a pedestrian (left, RCS is 2.37 dBSm) and a vehicle (right, RCS is 14.4 dBSm).

To confirm the general estimation performance, we simulate the proposed AIC radar estimation system 100 times at each angle pair with random phases. The estimated targets are also assumed to be a pedestrian and a vehicle. Figure 9 shows the standard error of the angle estimation using the proposed AIC radar system. The standard error is defined as

$$SE = \sqrt{\frac{1}{F}\Sigma_{f=1}^{F}\{(\theta_1'^{(f)} - \theta_1)^2 + (\theta_2'^{(f)} - \theta_2)^2\}} \qquad (8)$$

where F is the number of simulations and θ_1 and θ_2 are the true angles. $\theta_1'^{(f)}$ and $\theta_2'^{(f)}$ are the estimated results. Before AIC, we can see that the standard error is high and varies by the true angle pair. After AIC, the standard error decreases. When the true angles are larger than ±10°, the standard error becomes less than 1°. When the true angles are smaller than ±10°, the estimation performance degrades because of the radar's angle resolution.

Figure 10 gives the average received power difference between the larger target and the smaller target. We can see

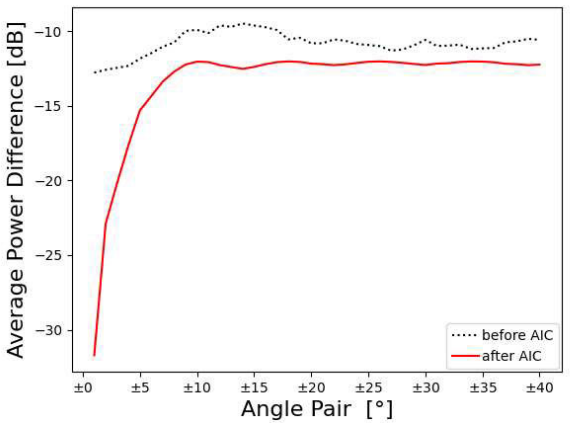

FIGURE 10. Average received power difference versus angle pair of the proposed AIC radar system when detecting a pedestrian (left, RCS is 2.37 dBSm) and a vehicle (right, RCS is 14.4 dBSm).

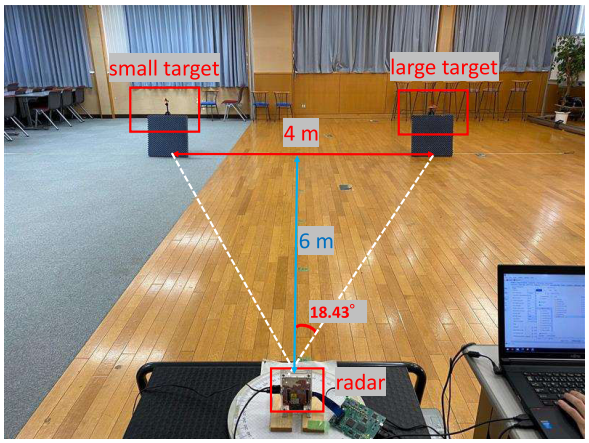

FIGURE 11. Experimental environment of estimating the angle and size of two different-sized targets.

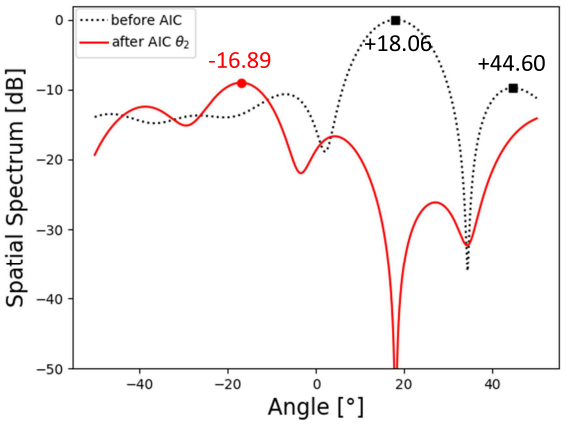

FIGURE 12. Experimental result of the proposed AIC radar system when detecting a 5 cm triangular pyramid reflector (left, RCS is 2.37 dBSm) and a 10 cm triangular pyramid reflector (right, RCS is 14.4 dBSm) at ±18.43° true angles.

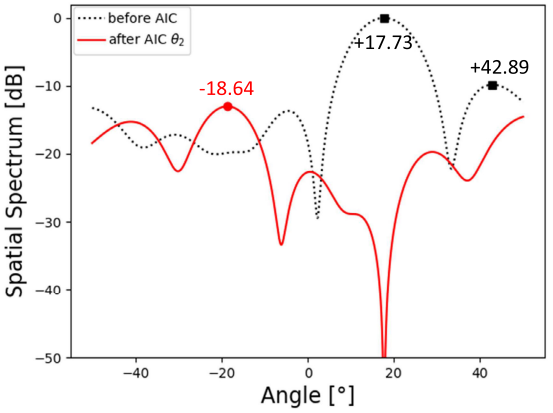

FIGURE 13. Experimental result of the proposed AIC radar system when detecting a 5 cm triangular pyramid reflector (left, RCS is 2.37 dBSm) and a 14 cm triangular pyramid reflector (right, RCS is 20.3 dBSm) at ±18.43° true angles.

that after AIC, the power difference converges to −12 dB (true amplitude ratio) when the true angles are larger than ±10°.

IV. EXPERIMENTAL RESULTS

Figure 11 shows the experimental environment. A TI-manufactured FMCW radar system (AWR1443) is used as the radar transceiver [39]. Its operating frequency is set to 77 GHz. The radar system uses two transmitting antennas and four-element receiver antennas. With the MIMO scheme, the receiver can be expanded to eight-element receiver antennas. The number of samples per chirp is 256 in the experiment. TI's default setting is adapted for the calibration of the MIMO radar system [40], [41]. Triangular pyramid reflectors of different sizes are used as targets. Their side lengths are 5 cm, 6 cm, 10 cm and 14 cm. Therefore, the RCSs of those targets are 2.37 dBSm, 5.53 dBSm, 14.4 dBSm, and 20.3 dBSm, as in the simulation in section III. The distance between the radar transceiver and the center of the two targets is set to 6 m. The distance between the two targets is 4 m. Thus, the true angles of the targets are ±18.43°. We change the distance between the two targets to adjust the angles of the targets.

Figure 12 depicts the experimental result of the proposed AIC radar system when detecting the 5 cm and 10 cm triangular pyramid reflectors as a pedestrian and a vehicle. Before AIC, the angles of the larger and smaller targets are estimated to be +18.06° and +44.60°, respectively. The angle of the smaller target cannot be estimated. After AIC, the angle of the smaller target is modified to −16.89°, and the received power difference is −9 dB. When calculated with the RCSs, the received power difference should be −12 dB, and the estimated angle of the smaller target should be −18.43° These errors occur due to three reasons. First, the reflective characteristics of the triangular pyramid reflectors vary with angles. The given RCSs are calculated when targets are set at 0°. Second, noise and discontinuity affect the performance of the MIMO radar system. Third, waves reflected by the floor affect the received power because the range resolution of the radar is approximately 50 cm. We confirm that the measured received power difference is the same, −9 dB, when each target is measured separately. Thus, this result is suitable.

Figure 13 depicts the experimental result of the proposed AIC radar system when detecting the 5 cm and 14 cm triangular pyramid reflectors as a pedestrian and a truck. We can see that pedestrian detection is very difficult. Before AIC, the angles of the larger and smaller targets are estimated to be +17.73° and +42.89°, respectively. The conventional system also cannot detect the smaller target. After AIC, the angle of the smaller target is modified to −18.64°, and the received power difference is −13 dB.

Figure 14 shows the experimental result of the proposed AIC radar system when detecting the 6 cm and 10 cm triangular pyramid reflectors as a bicycle and a vehicle, respectively. We can see that the influence of the larger target is also small

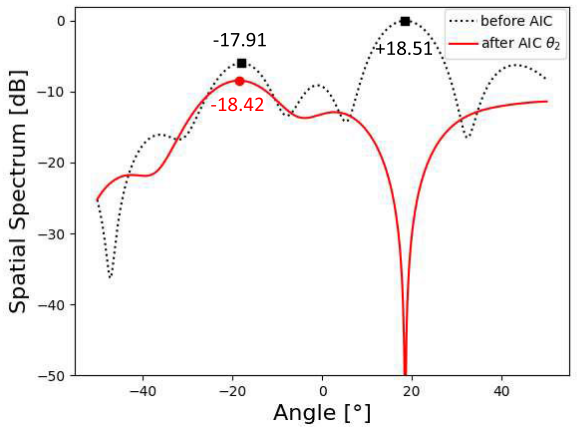

FIGURE 14. Experimental result of the proposed AIC radar system when detecting a 6 cm triangular pyramid reflector (left, RCS is 5.53 dBSm) and a 10 cm triangular pyramid reflector (right, RCS is 14.4 dBSm) at ±18.43° true angles.

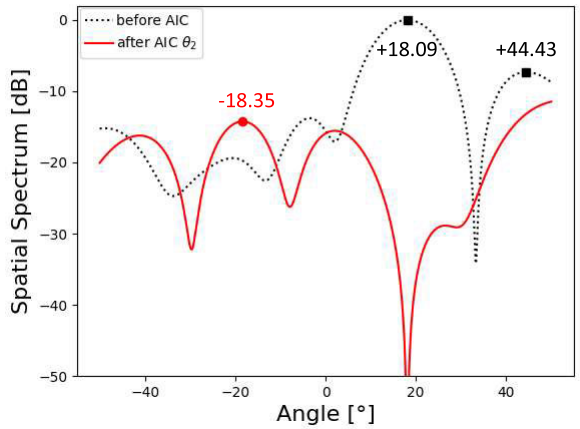

FIGURE 15. Experimental result of the proposed AIC radar system when detecting a 6 cm triangular pyramid reflector (left, RCS is 5.53 dBSm) and a 14 cm triangular pyramid reflector (right, RCS is 20.3 dBSm) at ±18.43° true angles.

due to a small RCS difference. Before AIC, the angles of the larger and smaller targets are estimated to be +18.51° and −17.91°, respectively. The conventional system also estimates the angle of the smaller target accurately. However, the received power difference is −5.9 dB with a 3 dB error (expected received power difference: 5.53 − 14.4 = −8.87 dB). After AIC, the angle of the smaller target is estimated to be −18.42°, and the received power difference is modified to −8.4 dB.

Figure 15 presents the experimental result of the proposed AIC radar system when detecting the 6 cm and 14 cm triangular pyramid reflectors as a bicycle and a truck, respectively. We can see that the bicycle detection becomes difficult contrary to the previous experimental result because the RCS difference is larger than that of Figure 14. Before AIC, the angles of the larger and smaller targets are estimated to be +18.09° and +44.43°, respectively. The conventional system cannot detect the smaller target. After AIC, the angle of the smaller target is modified to −18.35°, and the received power difference is −14.2 dB (expected received power difference: 5.53 − 20.3 = −14.77 dB).

The above four cases are representatives to show that the proposed AIC radar is effective in reducing the influence of sidelobes. For the other angle pairs (e.g., ±9.46, ±26.56, ±33.69), we also confirmed the good performances of the AIC scheme. Furthermore, we succeeded in the detection of three targets by the successive AIC scheme.

V. CONCLUSION

In this paper, we focus on estimating the angle and size of two different-sized targets: a pedestrian and a vehicle. Due to the influence of the sidelobes from the larger target, estimating the angle and size of the smaller targets was difficult with the conventional radar system. We proposed a novel scheme called AIC for reducing the influence of sidelobes. The performance of the proposed AIC radar system was evaluated through both computer simulations and experiments. The simulation results show that the proposed AIC radar system can estimate the angles of the targets within a 1-degree error, and the size estimation error is also 1 dB when the targets are set at distances longer than the radar resolution limit (±10°). The experimental results also show that the proposed AIC radar system is effective in detecting smaller targets that cannot be detected due to the sidelobes from the larger target. Furthermore, a successive AIC scheme for multiple targets (more than two) will be reported in the near future.

REFERENCES

[1] Z. Feng, M. Li, M. Stolz, M. Kunert, and W. Wiesbeck, "Lane detection with a high-resolution automotive radar by introducing a new type of road marking," *IEEE Trans. Intell. Transp. Syst.*, vol. 20, no. 7, pp. 2430–2447, Jul. 2019, doi: 10.1109/TITS.2018.2866079.

[2] J.-S. Kim, H.-J. Kim, M. Shin, J.-H. Park, O.-Y. Kwon, R. Song, S. Lee, S. Nam, and B.-S. Kim, "79 GHz active array FMCW radar system on low-cost FR-4 substrates," *IEEE Access*, vol. 8, pp. 213854–213865, 2020, doi: 10.1109/ACCESS.2020.3039513.

[3] X. Gao, G. Xing, S. Roy, and H. Liu, "Experiments with mmWave automotive radar test-bed," in *Proc. 53rd Asilomar Conf. Signals, Syst., Comput.*, Pacific Grove, CA, USA, Nov. 2019, pp. 1–6, doi: 10.1109/IEEECONF44664.2019.9048939.

[4] T.-Y. Lee, V. Skvortsov, M.-S. Kim, S.-H. Han, and M.-H. Ka, "Application of *W*-band FMCW radar for road curvature estimation in poor visibility conditions," *IEEE Sensors J.*, vol. 18, no. 13, pp. 5300–5312, Jul. 2018, doi: 10.1109/JSEN.2018.2837875.

[5] X. Yi, G. Feng, Z. Liang, C. Wang, B. Liu, C. Li, K. Yang, C. C. Boon, and Q. Xue, "A 24/77 GHz dual-band receiver for automotive radar applications," *IEEE Access*, vol. 7, pp. 48053–48059, 2019, doi: 10.1109/ACCESS.2019.2904493.

[6] D. Li, H. Lin, H. Liu, H. Wu, and X. Tan, "Focus improvement for squint FMCW-SAR data using modified inverse chirp-Z transform based on spatial-variant linear range cell migration correction and series inversion," *IEEE Sensors J.*, vol. 16, no. 8, pp. 2564–2574, Apr. 2016, doi: 10.1109/JSEN.2016.2521400.

[7] U. Chipengo, A. Sligar, and S. Carpenter, "High fidelity physics simulation of 128 channel MIMO sensor for 77 GHz automotive radar," *IEEE Access*, vol. 8, pp. 160643–160652, 2020, doi: 10.1109/ACCESS.2020.3021362.

[8] M.-S. Lee, "Signal modeling and analysis of a planar phased-array FMCW radar with antenna switching," *IEEE Antennas Wireless Propag. Lett.*, vol. 10, pp. 179–182, 2011, doi: 10.1109/LAWP.2011.2123074.

[9] J. M. GarcGarcíaa, D. Zoeke, and M. Vossiek, "MIMO-FMCW radar-based parking monitoring application with a modified convolutional neural network with spatial priors," *IEEE Access*, vol. 6, pp. 41391–41398, 2018, doi: 10.1109/ACCESS.2018.2857007.
[10] Z. Peng and C. Li, "A portable *K*-band 3-D MIMO radar with nonuniformly spaced array for short-range localization," *IEEE Trans. Microw. Theory Techn.*, vol. 66, no. 11, pp. 5075–5086, Nov. 2018, doi: 10.1109/TMTT.2018.2869565.
[11] P. Grüner, M. Geiger, and C. Waldschmidt, "Ultracompact monostatic MIMO radar with nonredundant aperture," *IEEE Trans. Microw. Theory Techn.*, vol. 68, no. 11, pp. 4805–4813, Nov. 2020, doi: 10.1109/TMTT.2020.3006055.
[12] M. Kucharski, A. Ergintav, W. A. Ahmad, M. Krstic, H. J. Ng, and D. Kissinger, "A scalable 79-GHz radar platform based on single-channel transceivers," *IEEE Trans. Microw. Theory Techn.*, vol. 67, no. 9, pp. 3882–3896, Sep. 2019, doi: 10.1109/TMTT.2019.2914104.
[13] H. Sim, S. Lee, S. Kang, and S.-C. Kim, "Enhanced DOA estimation using linearly predicted array expansion for automotive radar systems," *IEEE Access*, vol. 7, pp. 47714–47727, 2019, doi: 10.1109/ACCESS.2019.2910120.
[14] S. Kim, B.-S. Kim, Y. Jin, and J. Lee, "Extrapolation-RELAX estimator based on spectrum partitioning for DOA estimation of FMCW radar," *IEEE Access*, vol. 7, pp. 98771–98780, 2019, doi: 10.1109/ACCESS.2019.2930102.
[15] J. Yoon, S. Lee, S. Lim, and S.-C. Kim, "High-density clutter recognition and suppression for automotive radar systems," *IEEE Access*, vol. 7, pp. 58368–58380, 2019, doi: 10.1109/ACCESS.2019.2914267.
[16] M. Ash, M. Ritchie, and K. Chetty, "On the application of digital moving target indication techniques to short-range FMCW radar data," *IEEE Sensors J.*, vol. 18, no. 10, pp. 4167–4175, May 2018, doi: 10.1109/JSEN.2018.2823588.
[17] W.-H. Fang and L.-D. Fang, "Joint angle and range estimation with signal clustering in FMCW radar," *IEEE Sensors J.*, vol. 20, no. 4, pp. 1882–1892, Feb. 2020, doi: 10.1109/JSEN.2019.2949367.
[18] C. Will, P. Vaishnav, A. Chakraborty, and A. Santra, "Human target detection, tracking, and classification using 24-GHz FMCW radar," *IEEE Sensors J.*, vol. 19, no. 17, pp. 7283–7299, Sep. 2019, doi: 10.1109/JSEN.2019.2914365.
[19] X. Huang, J. Ding, D. Liang, and L. Wen, "Multi-person recognition using separated micro-Doppler signatures," *IEEE Sensors J.*, vol. 20, no. 12, pp. 6605–6611, Jun. 2020, doi: 10.1109/JSEN.2020.2977170.
[20] M. A. Tanha, P. V. Brennan, M. Ash, A. Kohler, and J. McElwaine, "Overlapped phased array antenna for avalanche radar," *IEEE Trans. Antennas Propag.*, vol. 65, no. 8, pp. 4017–4026, Aug. 2017, doi: 10.1109/TAP.2017.2712183.
[21] M. Porranzl, C. Wagner, H. Jaeger, and A. Stelzer, "On-wafer noise characterization of an automotive monostatic radar transceiver with self-interference evaluation," *IEEE Trans. Microw. Theory Techn.*, vol. 67, no. 8, pp. 3494–3505, Aug. 2019, doi: 10.1109/TMTT.2019.2916864.
[22] M. Porranzl, C. Wagner, H. Jaeger, and A. Stelzer, "High-bandwidth quasi-circulator-based monostatic automotive radar with self-interference suppression," *IEEE Trans. Microw. Theory Techn.*, vol. 69, no. 1, pp. 198–209, Jan. 2021, doi: 10.1109/TMTT.2020.3036007.
[23] D. Oh and J.-H. Lee, "Low-complexity range-azimuth FMCW radar sensor using joint angle and delay estimation without SVD and EVD," *IEEE Sensors J.*, vol. 15, no. 9, pp. 4799–4811, Sep. 2015, doi: 10.1109/JSEN.2015.2428814.
[24] J. Kim, S. Lee, Y.-H. Kim, and S.-C. Kim, "Classification of interference signal for automotive radar systems with convolutional neural network," *IEEE Access*, vol. 8, pp. 176717–176727, 2020, doi: 10.1109/ACCESS.2020.3026749.
[25] Y. Wang, A. Ren, M. Zhou, W. Wang, and X. Yang, "A novel detection and recognition method for continuous hand gesture using FMCW radar," *IEEE Access*, vol. 8, pp. 167264–167275, 2020, doi: 10.1109/ACCESS.2020.3023187.
[26] H. Sim, T.-D. Do, S. Lee, Y.-H. Kim, and S.-C. Kim, "Road environment recognition for automotive FMCW RADAR systems through convolutional neural network," *IEEE Access*, vol. 8, pp. 141648–141656, 2020, doi: 10.1109/ACCESS.2020.3013263.
[27] C. Ding, R. Chae, J. Wang, L. Zhang, H. Hong, X. Zhu, and C. Li, "Inattentive driving behavior detection based on portable FMCW radar," *IEEE Trans. Microw. Theory Techn.*, vol. 67, no. 10, pp. 4031–4041, Oct. 2019, doi: 10.1109/TMTT.2019.2934413.
[28] R. Sun, J. Sakai, K. Suzuki, J. Zheng, S. Takeda, M. Umehira, and H. Kuroda, "Proposal of antenna element space interference cancelling radar," in *Proc. Joint Indo-Jpn. Smart City Conf.*, Mar. 2021.
[29] S. Sen, N. Santhapuri, R. R. Choudhury, and S. Nelakuditi, "Successive interference cancellation: A back-of-the-envelope perspective," in *Proc. 9th ACM SIGCOMM Workshop Hot Topics Netw. (Hotnets)*, 2010, pp. 1–6.
[30] J. Park, B. Clerckx, J. Chun, and B. J. Jeong, "Lattice reduction-aided successive interference cancelation for MIMO interference channels," *IEEE Trans. Veh. Technol.*, vol. 63, no. 8, pp. 4131–4135, Oct. 2014, doi: 10.1109/TVT.2014.2302323.
[31] J. A. Högbom, "Aperture synthesis with a non-regular distribution of interferometer baselines," *Astron. Astrophys. Suppl. Ser.*, vol. 15, p. 417, Jun. 1974.
[32] G. Hislop, N. Sakar, and C. Craeye, "Direction finding with MUSIC and CLEAN," *IEEE Trans. Antennas Propag.*, vol. 61, no. 7, pp. 3839–3849, Jul. 2013, doi: 10.1109/TAP.2013.2255854.
[33] J. W. Choi and S. H. Cho, "A new multi-human detection algorithm using an IR-UWB radar system," in *Proc. 3rd Int. Conf. Innov. Comput. Technol. (INTECH)*, London, U.K., Aug. 2013, pp. 467–472, doi: 10.1109/INTECH.2013.6653718.
[34] P. C. Chang, R. J. Burkholder, and J. L. Volakis, "Adaptive CLEAN with target refocusing for through-wall image improvement," *IEEE Trans. Antennas Propag.*, vol. 58, no. 1, pp. 155–162, Jan. 2010, doi: 10.1109/TAP.2009.2036131.
[35] O. Akhdar, M. Mouhamadou, D. Carsenat, C. Decroze, and T. Monediere, "A new CLEAN algorithm for angle of arrival denoising," *IEEE Antennas Wireless Propag. Lett.*, vol. 8, pp. 478–481, 2009, doi: 10.1109/LAWP.2009.2014890.
[36] P. Berestesky and E. H. Attia, "Sidelobe leakage reduction in random phase diversity radar using coherent CLEAN," *IEEE Trans. Aerosp. Electron. Syst.*, vol. 55, no. 5, pp. 2426–2435, Oct. 2019, doi: 10.1109/TAES.2018.2888652.
[37] C. Pfeffer, R. Feger, C. Wagner, and A. Stelzer, "FMCW MIMO radar system for frequency-division multiple TX-beamforming," *IEEE Trans. Microw. Theory Techn.*, vol. 61, no. 12, pp. 4262–4274, Dec. 2013, doi: 10.1109/TMTT.2013.2287675.
[38] M. Jahn, R. Feger, C. Wagner, Z. Tong, and A. Stelzer, "A four-channel 94-GHz SiGe-based digital beamforming FMCW radar," *IEEE Trans. Microw. Theory Techn.*, vol. 60, no. 3, pp. 861–869, Mar. 2012, doi: 10.1109/TMTT.2011.2181187.
[39] S. Rao, "MIMO radar (rev. A)," Texas Instrum., Dallas, TX, USA, Appl. Rep. [Online]. Available: https://www.ti.com/lit/an/swra554a/swra554a.pdf
[40] A. Durr, R. Kramer, D. Schwarz, M. Geiger, and C. Waldschmidt, "Calibration-based phase coherence of incoherent and quasi-coherent 160-GHz MIMO radars," *IEEE Trans. Microw. Theory Techn.*, vol. 68, no. 7, pp. 2768–2778, Jul. 2020, doi: 10.1109/TMTT.2020.2971187.
[41] C. Zhang, M. Cao, Y. Gong, Y. Li, Y. Huang, and H. Wang, "Calibration of motional frequency spread for wide-band FMCW automotive millimeter-wave radar," *IEEE Access*, vol. 8, pp. 14355–14366, 2020, doi: 10.1109/ACCESS.2020.2966222.

RAN SUN (Member, IEEE) received the B.E., M.E., and Ph.D. degrees in computer and information science from Ibaraki University, in 2016, 2017, and 2020, respectively. Since 2020, he has been an Assistant Professor with Ibaraki University. His research interests include optical wireless communication, error correcting codes, the Internet of Things platform, and vehicle-borne radar. He is a member of IEICE.

JUNICHIROU SAKAI is currently with the Graduate School of Ibaraki University.

KOUHEI SUZUKI is currently with Ibaraki University.

JIAYING ZHENG is currently with Ibaraki University.

SHIGEKI TAKEDA (Member, IEEE) received the B.E., M.E., and Ph.D. degrees in electrical and electronic engineering from Tottori University, Tottori, Japan, in 1996, 1998, and 2000, respectively. Since 2000, he has been with the Department of Media and Telecommunications Engineering, College of Engineering, Ibaraki University, Japan, where he is currently a Professor. His research interests include RFID tags and antenna systems.

MASAHIRO UMEHIRA (Member, IEEE) received the B.E., M.E., and Ph.D. degrees from Kyoto University, Japan, in 1978, 1980, and 2000, respectively. In 1980, he joined Nippon Telegraph and Telephone Corporation (NTT), where he was engaged in the research and development of modem and TDMA equipment for satellite communications, TDMA satellite communication systems, broadband wireless access systems for mobile multimedia services, and ubiquitous wireless systems. From 1987 to 1988, he was with the Communications Research Center, Department of Communications, Canada, as a Visiting Scientist. Since 2006, he has been a Professor with Ibaraki University, Hitachi, and has been in the position of the Deputy Dean of the College of Engineering, Ibaraki University, since 2012. His research interests include broadband wireless access technologies, wireless networking and cognitive radio technologies for future fixed/nomadic/mobile wireless systems, future satellite communication systems, and ubiquitous services using wireless technologies. He is a Fellow of IEICE, Japan. He has served as the President for the IEICE Communications Society, Japan, in 2015. He received the Young Engineer Award and the Achievement Award from IEICE, in 1987 and 1999, respectively. He also received the Education, Culture, Sports, Science and Technology Minister Award, in 2001, and so on.

XIAOYAN WANG (Senior Member, IEEE) received the B.E. degree from Beihang University, China, and the M.E. and Ph.D. degrees from the University of Tsukuba, Japan. From 2013 to 2016, he worked as an Assistant Professor (by special appointment) with the National Institute of Informatics (NII), Japan. He is currently working as an Associate Professor with the Graduate School of Science and Engineering, Ibaraki University, Japan. His research interests include intelligent networking, wireless communications, cloud computing, big data systems, and security and privacy.

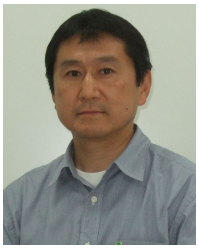

HIROSHI KURODA received the B.S. degree in electronic engineering from Kyoto University, in 1984, and the Ph.D. degree in engineering from the Tokyo Institute of Technology, in 2005. He is currently with Hitachi Astemo Ltd., Japan. He is also engaged in the development of the millimeter wave radar for automobile. He is a member of the Institute of Electronics, Information and Communication Engineers (IEICE) and the Society of Automotive Engineers of Japan (JSAE).